JOURNAL OF AIRCRAFT
Vol. 35, No. 1, January–February 1998

Unsteady Aeroelastic Optimization in the Transonic Regime

R. M. Kolonay*
U.S. Air Force Research Laboratory, Wright–Patterson Air Force Base, Ohio 45433
and
Henry T. Y. Yang†
University of California, Santa Barbara, Santa Barbara, California 93106

A methodology for including transonic flutter requirements in the preliminary automated structural design environment is developed and tested. The problem of minimizing structural weight while satisfying behavioral constraints is stated in nonlinear mathematical programming form and is solved using a gradient-based optimizing technique. The structure is modeled by using finite elements, and the associated design variables consist of the structural properties: thicknesses of skins, spars, and ribs; cross-sectional areas of posts and spar and rib caps; and concentrated masses. The method requires that the transonic unsteady aerodynamic forces be represented in the frequency or Laplace domain. In this work, the indicial response method is used to transform time-domain aerodynamic forces found by solving the transonic small disturbance (TSD) equations into the Laplace domain. The indicial responses are calculated about static aeroelastic equilibriums found using the TSD equations for the steady aerodynamics. Once in the Laplace domain, the unsteady aerodynamic forces are used to determine system dynamic stability by the *p*-method and in semianalytic equations for the flutter constraint sensitivities. With constraint values and the required gradients, a Taylor series approximation is used to develop an approximate nonlinear mathematical programming problem for weight minimization. This approximate optimization problem is iteratively solved by the method of modified feasible directions until convergence of the exact problem is obtained. Examples of the redesign methodology are given for the simultaneous consideration of constraints on transonic flutter, stresses, and displacements. Results found using nonlinear aerodynamics show that designs can differ considerably from those obtained using linear unsteady aerodynamics when in the transonic flight regime.

Introduction

THE missions of aeronautical and space vehicles of the future are becoming increasingly complex. Identifying trade-offs among pertinent disciplines has become more critical in producing vehicles that perform their prescribed missions. It has become difficult for the traditional methods to find a design that satisfies these requirements, let alone an optimal design. To satisfy this need, many software tools have recently been developed that are capable of generating integrated designs using formal mathematical optimization techniques.[1–8] For a given system, these tools determine system parameters (design variables) to minimize/maximize some system attribute(s) [objective function(s)] while the behavioral and/or performance requirements (constraints) of the system are met. Using such tools in the development of new systems enables engineers to obtain critical information early in the design so that informed choices can be made.

The focus of past work in multidisciplinary automated design concentrated on employing linear engineering analyses to determine system responses. The objective of this work is to develop and test a methodology for incorporating nonlinear analysis information into the multidisciplinary design environment. The methodology applies to engineering systems in which the system response is linear but the external loads are nonlinear and are functions of the system response. The specific application is to the area of transonic unsteady aeroelastic optimization. The purpose is to demonstrate the methodology by developing and testing the theoretical background for an algorithm that is capable of generating minimum weight designs of aircraft structures subject to flutter constraints in the transonic flight regime.

The unsteady aerodynamic theories used for past investigations concerning automated structural optimization and flutter constraints were linear. Methods such as the doublet lattice and strip theory for subsonic unsteady aerodynamics, and Mach box, strip theory, constant pressure method, and piston theory for supersonic aerodynamics, were employed. Use of nonlinear aerodynamics in optimization is a more recent development. This is because the nonlinear aerodynamic solution schemes themselves were a research topic throughout the 1970s and 1980s. Much of the work associated with automated design and nonlinear aerodynamics has been done with the use of computational fluid dynamics (CFD) methods linked with formal optimization techniques to determine aerodynamic parameters such as thickness-to-chord ratio, airfoil shape, and planform shape while minimizing or maximizing aerodynamic performances, e.g., drag or lift. Few works specifically associated with structural design subject to transonic flutter constraints were found in the literature.[9,10] In these works the authors calculated, by analytical as well as finite difference methods, the sensitivities of flutter speed with respect to structural parameters using transonic aerodynamics for a two-dimensional airfoil. The forms of the unsteady aerodynamics were the indicial response functions created by Leishman and Nguyen.[11] The structural parameters considered were those found in the two-degree-of-freedom aeroelastic equations of motion: mass ratio, static unbalance, radius of gyration, bending frequency, and torsional frequency. Although the sensitivities were found, no design studies were performed.

Approach

The problem of minimizing structural weight while satisfying behavioral constraints is stated in nonlinear mathematical

Received Oct. 9, 1996; revision received Aug. 25, 1997; accepted for publication Aug. 29, 1997.

*Aerospace Engineer, Structures Division, Flight Dynamics Directorate. Member AIAA.

†Professor and Chancellor, Department of Mechanical and Environmental Engineering. Fellow AIAA.

programming form and solved using a gradient-based optimizing technique. The structure is modeled using finite elements, and the associated design variables consist of structural properties: thicknesses of skins, spars, and ribs; cross-sectional areas of posts and spar and rib caps; and concentrated masses. The spars and ribs are assumed to be built-up, thin-walled cross sections, with the webs modeled by shear elements and one-dimensional membrane elements representing the posts and caps. In this research it is assumed that at a given static aeroelastic equilibrium position, the change in the dynamic angle of attack about that equilibrium is small. This assumption implies that the behavior of the aerodynamic forces and shock movement are linear with a change in the dynamic angle of attack. These assumptions enable time–domain computational fluid aerodynamics to be curve-fit into the Laplace domain.[12,13] For the present studies, the indicial response method (IRM) is used to transform time–domain aerodynamic forces found by solving the transonic small disturbance (TSD) equations into the Laplace domain. The indicial responses are calculated about static aeroelastic equilibriums found using the TSD equations for the steady aerodynamics. Once in the Laplace domain, the unsteady aerodynamics are used to determine system dynamic stability by the *p*-method and in semianalytic equations for the flutter constraint sensitivities. With constraint values and the required gradients, a Taylor series approximation (TSA) is used to develop an approximate nonlinear mathematical programming problem for weight minimization. This approximate optimization problem is iteratively solved by the method of modified feasible directions[14] until convergence of the exact problem is obtained.

Optimization Problem

The problem of minimum weight design can be stated in mathematical form as follows:

Minimize an objective function

$$F(\boldsymbol{v}) \tag{1}$$

subject to the constraint conditions

$$Z_j(\boldsymbol{v}) \leq \bar{Z}_j, \qquad j = 1, 2, \ldots, n, \qquad \boldsymbol{v}^L \leq \boldsymbol{v} \leq \boldsymbol{v}^U$$

where $F(\boldsymbol{v})$ is the weight of the structure, and $\boldsymbol{v}$ is a vector of design variables that relate directly to structural physical properties such as membrane thicknesses, rod and bar cross-sectional areas, and concentrated masses. The $Z_j(\boldsymbol{v})$ consist of all n behavioral constraints such as component stresses, structural displacements, and aeroelastic damping, and the values of $\bar{Z}_j$ are the given allowables for the $Z_j(\boldsymbol{v})$. In addition to the $Z_j(\boldsymbol{v})$, each $\boldsymbol{v}$ has upper bounds $\boldsymbol{v}^U$ and lower bounds $\boldsymbol{v}^L$, referred to as side constraints. Equation (1) represents the classical nonlinear mathematical programming problem.

The objective function for the present work is the structural weight of the system and is represented by

$$W = \sum_{i=1}^{nldv} \rho_{v_i} V_i(\boldsymbol{v}) \tag{2}$$

where W is the total designed structural weight of the system, ρ_{v_i} and $V_i(\boldsymbol{v})$ are the mass density and volume, respectively, of the ith structural element participating in the design. Note that the V_i can depend on more than one $\boldsymbol{v}$. The design variables are defined at two levels.[15]

Flutter Analysis and Constraint

Using the *p*-method for the flutter analysis, the fundamental equation of motion can be expressed as[15]

$$[(U_\infty/b)^2 p^2[\bar{M}] + (U_\infty/b)p[\bar{B}] + [\bar{K}] - \tfrac{1}{2}\rho_\infty U_\infty^2[\bar{Q}(p)]]\boldsymbol{q}(p) = 0 \tag{3}$$

Using the approximation for $[\bar{Q}(p)]$,[12,13] which employs the TSD theory along with the IRM, the generalized aerodynamic matrix $[\bar{Q}(p)]$ is expressed in terms of p as

$$[\bar{Q}(p)] = \bar{Q}_{ij}(p) = 4b^2 \sum_{r=1}^{n} 2p \left(\frac{C_{r_{ij}}}{2p + b_{r_{ij}}}\right) \tag{4}$$

where $C_{r_{ij}}$ and $b_{r_{ij}}$ are determined by curve-fitting time-domain indicial responses,[13] and the ij subscripts represent the ith row and jth column in the $[\bar{Q}(p)]$ matrix.

The flutter constraint is defined by satisfying requirements on modal damping at a series of velocities, rather than on the actual flutter speed.[2,15,16] This can be expressed as

$$(\gamma_{lj} \leq \gamma_{j\text{REQ}}) \text{ with } \begin{pmatrix} j = 1, 2, \ldots, \text{number of velocities} \\ l = 1, 2, \ldots, \text{number of modes} \end{pmatrix} \tag{5}$$

or

$$Z_j = \frac{\gamma_{lj} - \gamma_{j\text{REQ}}}{\text{GFACT}} \leq 0$$

where $\gamma_{j\text{REQ}}$ is the required level of damping at the jth velocity, and γ_{lj} is the calculated damping value for the lth mode at the jth velocity. The general normalization factor (GFACT) is used to scale the constraint value. GFACT must be used because normalization cannot be done by $\gamma_{j\text{REQ}}$, which can take on the value of 0. For this research, a value of 0.1 for GFACT is used in all cases studied.

Sensitivity of Flutter Constraint with Respect to Structural Design Variables

The derivative of the constraint in Eq. (5) with respect to $\boldsymbol{v}$ is

$$\frac{\partial Z_j}{\partial \boldsymbol{v}} = \frac{1}{\text{GFACT}} \frac{\partial \gamma_{lj}}{\partial \boldsymbol{v}} \tag{6}$$

Using the definition of p in Eq. (3) results in the following representation of γ. The subscripts on γ will be dropped from now on for simplicity of presentation

$$\gamma = (p/k) - i \tag{7}$$

Differentiating Eq. (7) with respect to v_s and realizing that γ is real, as well as $\partial\gamma/\partial\boldsymbol{v}$, yields

$$\frac{\partial \gamma}{\partial \boldsymbol{v}} = \frac{1}{k}\left[\frac{\partial}{\partial \boldsymbol{v}} \Re(p) - \gamma \frac{\partial}{\partial \boldsymbol{v}} \Im(p)\right] \tag{8}$$

The gradient of the eigenvalue p is found by differentiating Eq. (3). Using the approach for approximating unsteady TSD aerodynamics[17] yields

$$\frac{\partial p}{\partial \boldsymbol{v}} = \left[-p^2 \left(\frac{U_\infty}{b}\right)^2 \boldsymbol{y}^T \frac{\partial}{\partial \boldsymbol{v}}[\bar{M}]\boldsymbol{q} - p\left(\frac{U_\infty}{b}\right)\boldsymbol{y}^T \frac{\partial}{\partial \boldsymbol{v}}[\bar{B}]\boldsymbol{q} - \boldsymbol{y}^T \frac{\partial}{\partial \boldsymbol{v}}[\bar{K}]\boldsymbol{q} + \frac{1}{2}\rho_\infty U_\infty^2 (4b^2)\boldsymbol{y}^T \left[\sum_{l=1}^{m} \left(\frac{\partial}{\partial \omega_l}\bar{Q}[(p)]\right)\left(\frac{\partial \omega_l}{\partial \boldsymbol{v}}\right)\right]\boldsymbol{q}\right] \Bigg/ \left[2p\left(\frac{U_\infty}{b}\right)^2 \boldsymbol{y}^T[\bar{M}]\boldsymbol{q} + \left(\frac{U_\infty}{b}\right)\boldsymbol{y}^T[\bar{B}]\boldsymbol{q} - \frac{1}{2}\rho_\infty U_\infty^2 (4b^2)\boldsymbol{y}^T \frac{\partial}{\partial p}[\bar{Q}(p)]\boldsymbol{q}\right] \tag{9}$$

For the derivation of Eq. (9), the structural modes are assumed to be a basis for the system. With this assumption, the eigenvector matrix Φ, which is used to determine the generalized quantities, is considered invariant with respect to $\boldsymbol{v}$ and, thus, any terms associated with $\partial[\Phi]^T/\partial \boldsymbol{v}$, $\partial[\Phi]/\partial \boldsymbol{v}$ are assumed zero. This assumption is valid for small increments in $\boldsymbol{v}$. The more modes retained for representing the basis of the system, the larger the changes allowed in $\boldsymbol{v}$. All terms in Eq. (9) can be found analytically, except for the term $\partial[\bar{Q}(p)]/\partial\omega_k$, which must be determined numerically. Reference 17 provides a discussion concerning the computation of this term using forward finite differences and its impact on the sensitivity calculations for some test cases.

Redesign Algorithm

After the engineering and sensitivity analyses are complete, the system can be redesigned. This is accomplished by solving the nonlinear mathematical programming problem stated in Eq. (1). For the present studies, the method of modified feasible directions (MMFD) (Ref. 14) is used to solve the optimization problem. Gradient-based optimization routines such as the MMFD require tens and sometimes hundreds of objective-function, objective-function-gradient, constraint, and constraint-gradient evaluations to obtain an optimal design. In the context of this work, the constraint evaluation (flutter-damping determination) and the constraint-gradient calculations are computationally expensive. These evaluations require a finite element eigenvalue analysis and several TSD time integrations. With these points in mind, it is wise to adopt approximate analysis and gradient techniques when performing the optimization. Therefore, an explicit first-order approximation is used. In particular, a first-order TSA is implemented.[18] The actual implementation used is that found in ASTROS (Ref. 15). It is the approximate problem that is submitted to the optimizer. Therefore, when the optimizer requires the objective function or constraints (evaluations or gradients), the approximations are used to satisfy the request. This communication between the approximate problem and the optimizer is termed an inner-loop iteration. When the approximate problem is solved and detailed, engineering analyses and sensitivity analyses are performed to construct a new approximate problem; it is referred to as an outer-loop iteration. When using approximations, it is important to realize that they are only accurate for small increments in v_s. This generates the requirement that move limits (MOVLIM) be imposed on the design variables of the following form:

$$\boldsymbol{v}_o/\text{MOVLIM} \leq \boldsymbol{v} \leq \text{MOVLIM} \cdot \boldsymbol{v}_o \qquad (10)$$

In the current studies, MOVLIM values varied from 1.01 to 2.0, depending on the problem and the iteration.

The procedure to perform the redesign follows.

1) Select a Mach number, corresponding velocity, altitude, and angle of attack.

2) With the dynamic pressure specified in step 1, a nonlinear static aeroelastic equilibrium is calculated. Here, the TSD program CAP-TSD (Ref. 19) is used for these calculations.

3) From the static aeroelastic equilibrium, indicial responses for the current set of design variables and associated mode shapes are determined. Again, CAP-TSD is used to provide the TSD unsteady aerodynamics.

4) Once the indicial responses are obtained, the Lapace domain unsteady aerodynamics can be determined and the flutter damping constraints and sensitivities evaluated.

5) With the results of step 4, an approximate problem is formulated and redesign takes place, yielding a new set of design variables that, in turn, produces new structural frequencies and mode shapes.

6) With the new set of design variables, steps 2-5 are repeated until a converged optimum is obtained. At the optimum, one normalized constraint must fall in the range $-1.5000 \times 10^{-3} \leq Z_j \leq 1.000 \times 10^{-3}$, and the total objective function cannot have moved by more than 1% from the previous iteration.

Design Examples

To demonstrate the preceding derivations, two wing models are considered at various flight conditions. The first is a rectangular, unswept, untapered planform that uses a beam representation for the structure. The second is a swept, tapered fighter planform, where the structure is represented by a built-up finite element wing box. Because the small disturbance meshes differ from the structural meshes, transformation of the mode shapes from the structural mesh to the CFD grid is required. In both cases, this is accomplished by using the infinite plate spline method.[20] For all of the TSD computations, a Cray Y-MP8/8128 (YMP) is employed, which has eight processors with a peak performance of 2.7 Gflops and 128 Mwords of core memory. Some computer resource usage is reported on these examples with the intent of presenting a rough order-of-magnitude estimate on the time necessary to perform the calculations, and to provide a basis of comparison for the different computations done within the present research. Also, for comparison purposes, designs are determined using both linear and nonlinear unsteady aerodynamics. For consistency, the linear cases are performed by employing the linear option in CAP-TSD, along with the IRM, to determine the linear unsteady aerodynamic forces.

Description of Rectangular Wing Example

The rectangular wing selected was used in Ref. 21 to demonstrate transonic flutter predictions. The wing has a moderate aspect ratio, a 6% parabolic airfoil, and a uniform cantilever beam representing the structural model (Fig. 1). Structural parameters, calculated natural frequencies, and modal descriptions are as follows: mass = 11.19 slugs/ft, torsional moment of inertia I = 29.14 slug-ft^2/ft, static unbalance S = 6.71 slug-ft/ft, bending stiffness EI = 23.65E+6 lb-ft^2, torsional stiffness GJ = 2.39E+6 lb-ft^2, mode 1 (first bending) 1.98 Hz, mode 2 (first torsion) 3.92 Hz. To evaluate the performance of the design methodology, it is assumed that the main structural beam is rectangular and it serves no aerodynamic purpose. To specify a rectangular cross section enables one to study in more detail the effect of specific geometric parameters such as height and width. However, whereas physically the beam cross

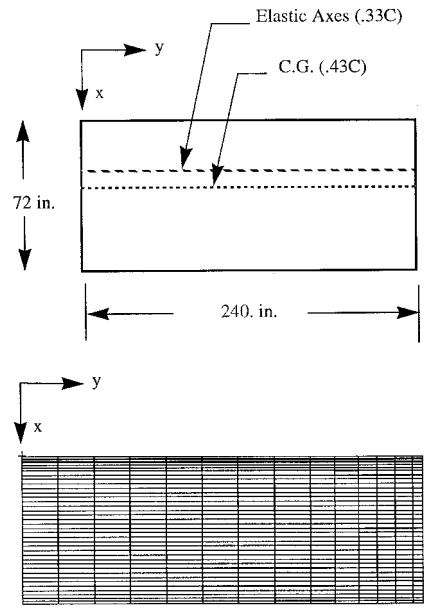

Fig. 1 Rectangular wing planform and CFD mesh (39 × 15 on wing).

section should be enclosed by the 6% parabolic airfoil, mathematically it is assumed that the beam section can extend beyond the airfoil configuration. This is necessary to match the *EI* and *GJ* distributions given in Ref. 21.

Rectangular Wing Design Case 1: M_∞ = 0.70, α_0 = 0.0 deg, Flutter Constraints

The first design condition chosen is *M* 0.70, U_∞ = 781 ft/s, and initial angle of attack α_0 = 0.0 deg, with flutter constraints only. The wing is designed using both linear and nonlinear unsteady aerodynamics. This case is chosen at a flight condition in which both the linear and nonlinear aerodynamics should yield the same results. The small disturbance model (Fig. 1) consists of a 60 × 23 × 40 mesh with 39 chordwise grids and 15 spanwise grids on the wing. The two design variables selected for the wing are the height and width of the beam, which serves as the main and only spar for the wing. Assuming a rectangular cross section, the initial width ($v_{1\,\text{initial}}$) and height ($v_{2\,\text{initial}}$) of the section are found to be 0.2590 and 0.9092 ft, respectively. These dimensions extend beyond the 6% parabolic airfoil used for the wing because of the selection of a rectangular cross section of the main structural beam, which serves no aerodynamic purpose.

For the purpose of comparing the results obtained using linear vs nonlinear unsteady aerodynamics, the altitude is not chosen arbitrarily. The densities used are those found by performing a time integration flutter analysis at M_∞ = 0.70, U_∞ = 781 ft/s, and α_0 = 0.0 deg, with linear and nonlinear aerodynamics. The flutter quantities found using CAP-TSD (Ref. 19) for the linear and nonlinear aerodynamics, respectively, are $\rho_{fTl\infty} \approx$ 6.288E−4 slugs/ft^3, $\omega_{fTl} \approx$ 2.33 Hz; and $\rho_{fTnl\infty} \approx$ 6.353E−4 slugs/ft^3, $\omega_{fTnl} \approx$ 2.33 Hz. With these densities the IRM approximate flutter quantities are found to be $U_{fIl} \approx$ 790 ft/s, $\omega_{fIl} \approx$ 2.33 Hz; and $U_{fInl} \approx$ 789 ft/s, $\omega_{fInl} \approx$ 2.33 Hz. The flutter constraint specified for design is a 20% increase in the flutter velocity obtained by the IRM (U_{fI}). Therefore, for the linear case, a constraint on damping of all *j* modes is required to be $\gamma_j \le 0.0$ for $U_{fIl} \le$ 948 ft/s and, for the nonlinear case, $\gamma_j \le 0.0$ for $U_{fInl} \le$ 947 ft/s. The redesign process is able to increase U_f by the required 20% and requires 11 detailed analyses (approximately 1 h of YMP CPU time) to converge for both cases (linear and nonlinear unsteady aerodynamics). Because the flight condition is inherently linear, both cases converge to the same final design, as expected. The final objective function increases by 16% ($v_{1\,\text{final}}$ = 0.2831 ft, $v_{2\,\text{final}}$ = 0.9651 ft, $\omega_{f\text{final}} \approx$ 2.68 Hz), indicating that a weight penalty is incurred to satisfy the flutter constraint. Figure 2 is a comparison of the initial and final linear and nonlinear $U_\infty - g$ curves. Here the increase in flutter velocity from the initial to the final design can be seen, along with the fact that the flutter mechanism does not change from the initial design. It is important to note that, for this example, the aerodynamic forces are updated at every other outer-loop iteration, and the nonlinear term in the damping constraint sensitivities $[\partial[\bar{Q}(p)]/\partial\omega_l$ in Eq. (9)] is found to contribute little to the gradient terms. The nonlinear term is thus excluded from the calculations. This example case, although simple, verifies that the design methodology is performing properly.

Rectangular Wing Design Case 2: M_∞ = 0.85, α_0 = 0.5 deg, Flutter Constraints

The flutter quantities determined for M_∞ = 0.85, U_∞ = 948 ft/s, α_0 = 0.5 deg using time integration (CAP-TSD) are $\rho_{fTl\infty} \approx$ 2.465E−4 slugs/ft^3, $\omega_{fTl} \approx$ 2.14 Hz; and $\rho_{fTnl\infty} \approx$ 1.910E−4 slugs/ft^3, $\omega_{fTnl} \approx$ 2.10 Hz. Using these densities, static aeroelastic equilibrium states are calculated. Figure 3 shows pressure coefficients for the upper surface C_p^U and lower surface C_p^L, and the difference between upper and lower surfaces ΔC_p, at the 27% spanwise location for the states of static aeroelastic equilibrium. The nonlinear static aeroelastic pressure coefficients indicate a shock developing on the upper surface of the wing at about 60% chord for this flight condition. The differences in flutter densities (or altitudes) and the pressure distributions clearly indicate that nonlinear effects are significant for this case. Using the static aeroelastic equilibriums, indicial responses for the first two fundamental modes are calculated, and these results are used to determine the approximate flutter parameters by the IRM. The results of the IRM flutter for the initial design ($v_{1\,\text{initial}}$ = 0.2590 ft, $v_{2\,\text{initial}}$ = 0.9092 ft) for both linear and nonlinear unsteady aerodynamics are found in Fig. 4 ($U_{fIl\infty} \approx$ 911 ft/s, $\omega_{fIl} \approx$ 2.10 Hz; $U_{fInl\infty} \approx$ 899 ft/s, $\omega_{fInl} \approx$ 2.07 Hz). Note that although the flutter mechanisms are the same for the linear and nonlinear unsteady aerodynamics, the flutter dynamic pressure differs by 25%. Also, examining the $U_\infty - g$ diagram in Fig. 4 shows that the nonlinear case crosses the axis at a much smaller slope than the linear case. For redesign, an increase of 20% is again set for the $U_{fI\infty}$. At the first constraint evaluation the linear case has a maximum constraint violation of 10.5%, where the nonlinear case has a maximum constraint violation of 3.9%. Both cases yield converged designs that satisfy the flutter constraint. When using nonlinear unsteady aerodynamics, the optimization converges in three iterations, using approximately 20 min of YMP CPU time, to a final weight 2.7% higher than the initial design ($v_{1\,\text{final}}$ = 0.26421 ft, $v_{2\,\text{final}}$ = 0.91609 ft, $\omega_{f\text{final}}$ = 2.17 Hz). When using linear unsteady aerodynamics, the optimization converges in seven iterations to a final weight 6.7% higher than the initial design ($v_{1\,\text{final}}$ = 0.27105 ft, $v_{2\,\text{final}}$ = 0.92747 ft, $\omega_{f\text{final}}$ = 2.27 Hz). The differences in the final design indicate the effects of using the nonlinear unsteady aerodynamics. Figure 4 shows the $U_\infty - g$ diagram for the final designs. Although the flutter mechanisms are the same, the flutter

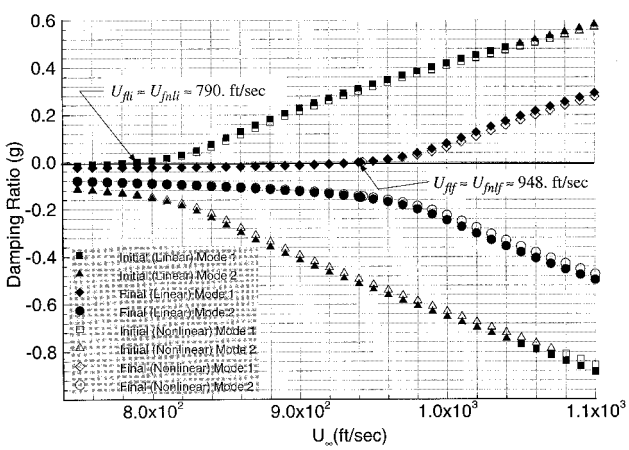

Fig. 2 Rectangular wing initial and final designs U_∞ vs *g*. M_∞ = 0.70, α_0 = 0.0 deg.

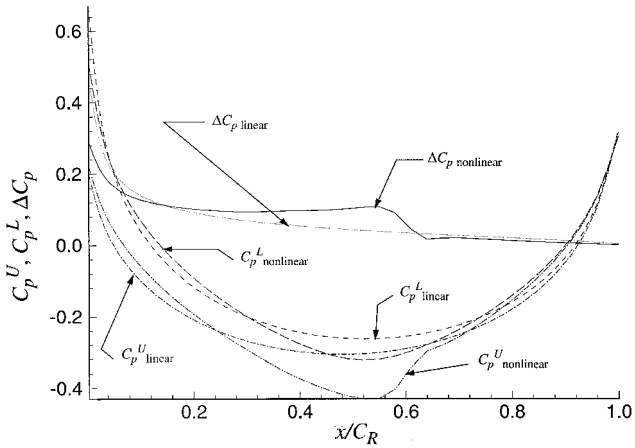

Fig. 3 Rectangular wing pressure coefficients at 27% span. M_∞ = 0.85, α_0 = 0.5 deg.

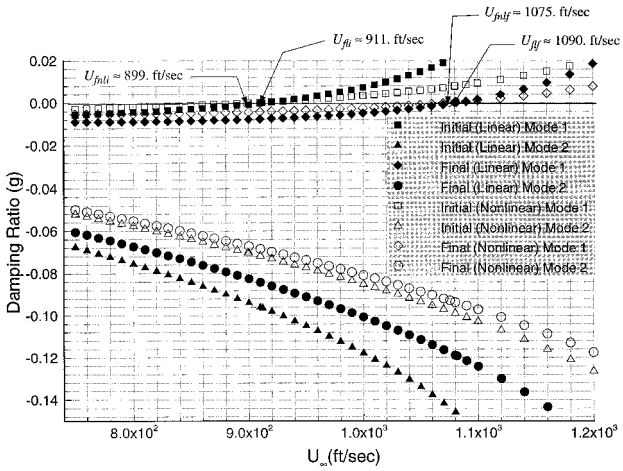

Fig. 4 Rectangular wing initial and final designs U_∞ vs g. M_∞ = 0.85, α_0 = 0.5 deg.

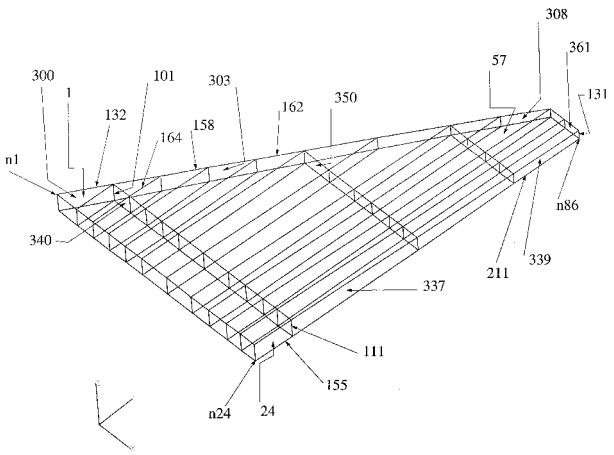

Fig. 5 Fighter wing finite element model.

frequencies differ by about 4%. Once again, the unsteady aerodynamics were updated at every other exact problem evaluation. Also, the nonlinear term in the damping sensitivity is determined to be negligible and is not included in the sensitivity calculations.

Description of Fighter Wing Example

This test case is a modified version of the sample case found in Ref. 22. For this work, the wing structure is terminated at the wing root (no carry-through attachment) and the overall mass is scaled to obtain the desired natural frequencies. In addition, a 4% parabolic airfoil is employed over the entire wing to include thickness effects. Figure 5 shows the finite element model with the node and element numbering schemes, and Fig. 6 shows the small disturbance finite difference mesh.

Here the first four natural vibration modes are used in the analyses. The frequencies for these modes are 5.62, 19.28, 24.12, and 36.83 Hz, respectively. The design variable linking scheme (adopted from Ref. 22), initial global design variables, initial physical variables, and minimum/maximum global design variables are given in Table 1. The initial designed weight of the wing box is 497.69 lb, with a total weight of the system being 4857.69 lb. Three cases are examined. The first is at a supersonic Mach number with only flutter constraints, using both linear and nonlinear unsteady aerodynamics. The second case is at a subsonic Mach number with only flutter constraints; again, both linear and nonlinear unsteady aerodynamics are used. The final case is at a subsonic Mach number with flutter, stress, and displacement constraints, using only nonlinear unsteady aerodynamics.

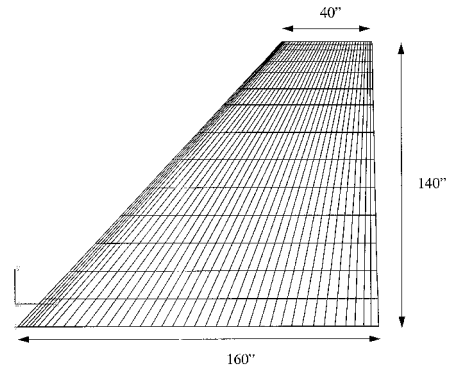

Fig. 6 Fighter wing CFD mesh (39 × 15 on wing) and planform.

Fighter Wing Case 1: M_∞ = 1.1, α_0 = 1.0 deg, Flutter Constraints

The flutter quantities calculated by time integration for the flight condition of M_∞ = 1.1, α_0 = 1.0 deg, and U_∞ = 14,736 in./s are $\rho_{fI} \approx$ 3.776E−7 lbf s^3/in., $\omega_{fI} \approx$ 19.48 Hz; and $\rho_{fInl} \approx$ 4.927E−7 lbf s^3/in., $\omega_{fInl} \approx$ 20.12 Hz. Using these densities, static aeroelastic equilibriums are found. Figure 7 shows the pressure coefficients at the 68% spanwise location for the static aeroelastic equilibriums. The differences in flutter densities and the pressure distributions indicate that nonlinear effects are present for this case. Using the static aeroelastic equilibriums, indicial responses are calculated, and these results are used to determine the approximate flutter parameters by the IRM. The results of the IRM flutter for the initial design for both linear and nonlinear unsteady aerodynamics are $U_{fI} \approx$ 14,705 in./s, $\omega_{fI} \approx$ 19.50 Hz; and $U_{fInl} \approx$ 14,751 in./s, $\omega_{fInl} \approx$ 20.07 Hz. Although the flutter mechanisms are the same for the linear and nonlinear unsteady aerodynamics, the flutter dynamic pressures differ by about 26%. Figure 8 shows the $U_\infty - g$ diagram associated with the mode of instability (mode 2) for the initial designs. The design requirement is to increase the flutter velocity by 20%. At the first constraint evaluation, the linear case has a maximum constraint violation of 92.6%, where the nonlinear case has a maximum constraint violation of 77.80%. Updating the unsteady aerodynamics at every other approximate problem definition (outer-loop iteration), and excluding the nonlinear gradient term, both cases are able to resize the structure to satisfy the 20% increase in the flutter velocity. When using linear unsteady aerodynamics, the optimization converges in 21 outer-loop iterations to a final designed weight of 566.3 lb (a 13.8% increase from the initial design). When using nonlinear unsteady aerodynamics, the optimization converged in 26 outer-loop iterations (6 h YMP CPU time) to a final designed weight of 464.51 lb (6.7% decrease from the initial design). Table 2 contains the final designs for both cases, indicating a significant difference in sizing and material distribution between the two final designs. The differences in the final design indicate the effects of using the nonlinear unsteady aerodynamics. The majority of the designed weight difference is accounted for by the root v_{15} and first-bay v_{16} skins. The linear design results in v_{15} and v_{16} being heavier than the nonlinear design by approximately 70 and 50 lb, respectively. Some of the differences in the distribution of material can also be attributed to the fact that, for the linear case, many of the design variables reach their maximum allowable values. This forces the optimizer to satisfy the constraint by using members that are less efficient in effecting the constraints. Figure 8 shows the $U_\infty - g$ diagram for the final designs for both the linear and nonlinear unsteady aerodynamic cases. These indicate a nice shift of the mode of instability (mode 2) to satisfy the constraint and that the flutter mechanism is the same as the initial design, with most of the changes occurring in the higher frequency modes. If linear unsteady aerodynamics are used, the system appears to be overdesigned and costs an additional 22% in designed weight.

Table 1 Fighter wing design variable linking, initial, minimum, and maximum values

Global design variable	Local design variable	Initial property value	Initial global value	Minimum global value	Maximum global value
1	CROD 101–131	0.05 in.^{2}	1.00	0.10	1.00
2	CSHEAR 309, 310, 312, 314, 316, 318, 312, 324, 328, 332	0.075 in.	1.00	0.25	1.50
3	CSHEAR 311, 313, 315, 317, 319, 322, 325, 329, 333	0.065 in.	1.00	0.25	1.50
4	CSHEAR 320, 323, 326, 330, 334	0.05 in.	1.00	0.25	1.50
5	CSHEAR 327, 331, 335	0.03 in.	1.00	0.25	1.50
6	CROD 134–153	1.00 in.^{2}	1.00	0.10	1.25
7	CROD 164–181	0.75 in.^{2}	1.00	0.10	1.25
8	CROD 188–197	0.60 in.^{2}	1.00	0.10	1.25
9	CROD 204–209	0.50 in.^{2}	1.00	0.10	1.25
10	CSHEAR 340–361	0.08 in.	1.00	0.25	1.50
11	CTRMEM 1, 2	0.25 in.	1.00	0.10	1.50
12	CTRMEM 23, 24	0.188 in.	1.00	0.10	1.50
13	CTRMEM 43, 44	0.08 in.	1.00	0.10	1.50
14	CTRMEM 55, 56	0.04 in.	1.00	0.10	1.50
15	CQDMEM1 3–22	0.25 in.	1.00	0.10	1.50
16	CQDMEM1 25–42	0.188 in.	1.00	0.10	1.50
17	CQDMEM1 45–54	0.08 in.	1.00	0.10	1.50
18	CQDMEM1 57–62	0.04 in.	1.00	0.10	1.50
19	CSHEAR 300, 336	0.135 in.	1.00	0.25	1.50
20	CSHEAR 301–304, 337	0.12 in.	1.00	0.25	1.50
21	CSHEAR 305, 306, 338	0.09 in.	1.00	0.25	1.50
22	CSHEAR 307, 308, 339	0.05 in.	1.00	0.25	1.50
23	CROD 132, 133, 154, 155	1.75 in.^{2}	1.00	0.10	1.25
24	CROD 156–163, 182, 183	1.35 in.^{2}	1.00	0.10	1.25
25	CROD 184–187, 198, 199	1.05 in.^{2}	1.00	0.10	1.25
26	CROD 200–203, 210, 211	0.88 in.^{2}	1.00	0.10	1.25

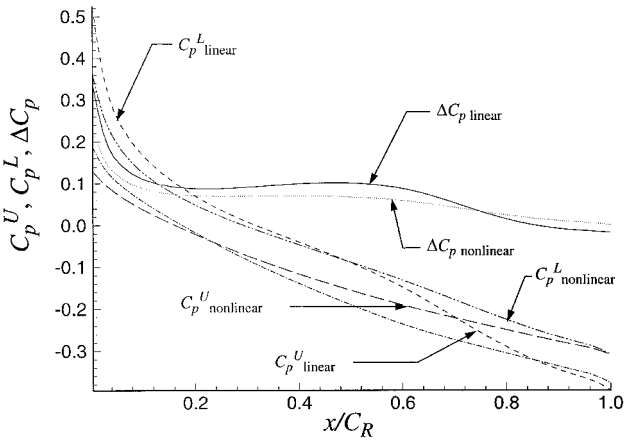

Fig. 7 Fighter wing aeroelastic pressure coefficients at 68.0% span. $M_\infty = 1.1$, $\alpha_0 = 1.0$ deg.

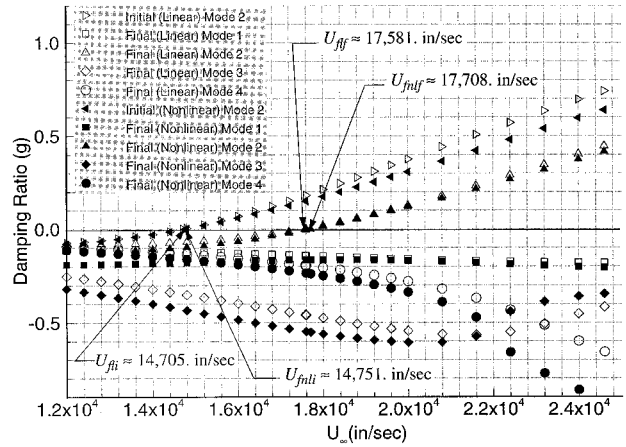

Fig. 8 Fighter wing linear and nonlinear final design U_∞ vs g. $M_\infty = 1.1$, $\alpha_0 = 1.0$ deg.

The only conclusion that can be reached at this time is that different designs will result if using linear vs nonlinear unsteady aerodynamics. Not only will the sizes differ but so, too, will the distribution of material. This is important because it implies one cannot take a linear design distribution and simply scale it to satisfy the nonlinear flutter constraint. It also implies that simply because a linear design may be heavier and appear to be conservative, a nonlinear analysis must be performed to verify that the nonlinear flutter constraint is satisfied. Even if the nonlinear analysis indicates that the flutter requirements are satisfied, there is no way to determine the weight penalty incurred by adopting the linear design.

Fighter Wing Case 2: $M_\infty = 0.93$, $\alpha_0 = 0.5$ deg, Flutter Constraints

Using time integration for the flight condition of $M_\infty = 0.93$, $\alpha_0 = 0.50$ deg, and $U_\infty = 12{,}459$ in./s, the flutter densities and frequencies are found to be $\rho_{fTl\infty} \approx 6.764\text{E}{-7}$ lbf s^3/in., $\omega_{fTl} \approx 19.73$ Hz; and $\rho_{fTnl\infty} \approx 6.571\text{E}{-7}$ lbf s^3/in., $\omega_{fTnl} \approx 19.52$ Hz. With these results, static aeroelastic equilibriums are determined. Figure 9, which shows the pressure coefficients at the 68% spanwise location for the static aeroelastic equilibriums, indicates a shock on both the upper and lower surfaces of the wing for the nonlinear aerodynamics. Although the flutter dynamic pressures differ by less than 3%, the pressure distributions indicate a considerable nonlinearity in the problem. Using the static aeroelastic equilibriums, indicial responses are calculated and used to determine the approximate flutter parameters by the IRM. The results of the IRM flutter for the initial design for both linear and nonlinear unsteady aerodynamics are $U_{fIl} \approx 12{,}492$ in./s, $\omega_{fIl} \approx 19.72$ Hz; and $U_{fInl} \approx 12{,}137$ in./s, $\omega_{fInl} \approx 19.64$ Hz. Figure 10 shows the $U_\infty - g$ diagram associated with the mode of instability (mode 2) for the initial designs. Once again, a 20% increase on the flutter velocity U_{fI} is desired during the redesign. At the first constraint evaluation, the linear case has a maximum constraint violation of 96.20%, where the nonlinear case has a maximum constraint violation of 95.04%. Both cases are able to resize the structure to satisfy the flutter constraint. When using linear

Table 2 Fighter wing linear and nonlinear final designs for flutter constraints[a]

Global design variable	Local design variable	Linear final physical value	Nonlinear final physical value	% difference between linear and nonlinear
1	CROD 101–131	0.024 in.^{2}	0.029 in.^{2}	+18.17
2	CSHEAR 309, 310, 312, 314, 316, 318, 312, 324, 328, 332	0.035 in.	0.039 in.	+10.13
3	CSHEAR 311, 313, 315, 317, 319, 322, 325, 329, 333	0.030 in.	0.033 in.	+10.19
4	CSHEAR 320, 323, 326, 330, 334	0.075 in.	0.028 in.	−62.29
5	CSHEAR 327, 331, 335	0.045 in.	0.052 in.	+15.23
6	CROD 134–153	0.467 in.^{2}	0.512 in.^{2}	+9.76
7	CROD 164–181	0.630 in.^{2}	0.385 in.^{2}	+38.94
8	CROD 188–197	0.750 in.^{2}	0.757 in.^{2}	+0.89
9	CROD 204–209	0.625 in.^{2}	0.706 in.^{2}	+12.88
10	CSHEAR 340–361	0.120 in.	0.134 in.	+11.26
11	CTRMEM 1, 2	0.117 in.	0.128 in.	+9.88
12	CTRMEM 23, 24	0.088 in.	0.096 in.	+9.80
13	CTRMEM 43, 44	0.041 in.	0.041 in.	+0.31
14	CTRMEM 55, 56	0.060 in.	0.068 in.	+13.10
15	CQDMEM1 3–22	0.375 in.	0.128 in.	−65.78
16	CQDMEM1 25–42	0.282 in.	0.217 in.	−22.92
17	CQDMEM1 45–54	0.120 in.	0.126 in.	+4.97
18	CQDMEM1 57–62	0.060 in.	0.068 in.	+12.81
19	CSHEAR 300, 336	0.203 in.	0.229 in.	+12.94
20	CSHEAR 301–304, 337	0.180 in.	0.203 in.	+12.73
21	CSHEAR 305, 306, 338	0.135 in.	0.107 in.	−20.65
22	CSHEAR 307, 308, 339	0.075 in.	0.086 in.	+15.22
23	CROD 132, 133, 154, 155	2.188 in.^{2}	2.421 in.^{2}	+23.34
24	CROD 156–163, 182, 183	0.630 in.^{2}	0.692 in.^{2}	+6.24
25	CROD 184–187, 198, 199	1.313 in.^{2}	1.284 in.^{2}	+2.15
26	CROD 200–203, 210, 211	1.100 in.^{2}	1.239 in.^{2}	+12.63

[a]$M_\infty = 1.1$, $\alpha_0 = 1.0$ deg

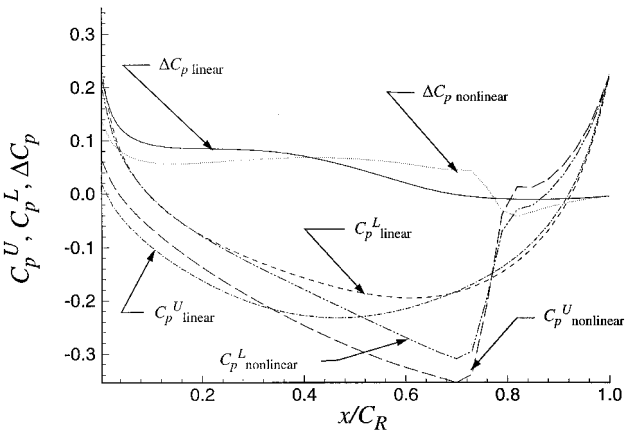

Fig. 9 Fighter wing aeroelastic pressure coefficients at 68.0% span. $M_\infty = 0.93$, $\alpha_0 = 0.5$ deg.

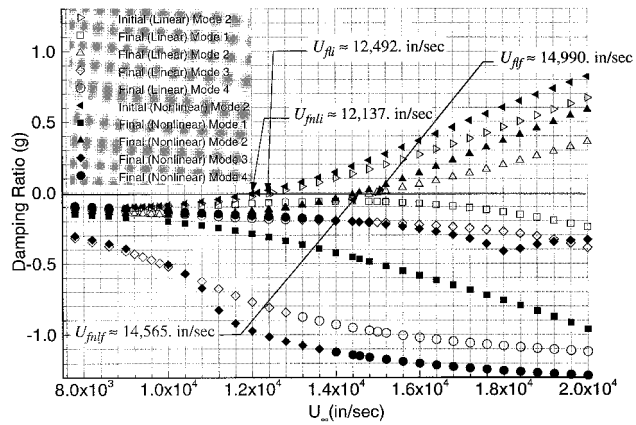

Fig. 10 Fighter wing linear and nonlinear final design U_∞ vs g. $M_\infty = 0.93$, $\alpha_0 = 0.5$ deg.

unsteady aerodynamics, the optimization converges in 15 outer-loop iterations to a final designed weight of 506.98 lb, a 1.87% increase from the initial design. When using nonlinear unsteady aerodynamics, the optimization also converges in 15 outer-loop iterations and 3 h of YMP CPU time to a final designed weight of 426.91 lb, a 14.22% decrease from the initial design. Table 3 contains the final designs for both cases. This table shows a difference between the two final designs in sizing and shows that for both designs many of the variables reached their minimum or maximum values. The largest difference in the sizing occurs at v_{15}. The nonlinear-design root skins are almost 80 lb lighter than the linear designs. Figure 10 shows the $U_\infty - g$ plots for the final designs for both the linear and nonlinear unsteady aerodynamic cases. Once again, one can observe a nice shift of the mode of instability (mode 2) to satisfy the constraint and that the flutter mechanism is the same as the initial design. If linear unsteady aerodynamics are used, the system appears to be overdesigned and costs an additional 18.75% in designed weight. This example again demonstrates that a different design results when using nonlinear vs linear unsteady aerodynamics. This is evident in Fig. 10, which indicates a rather significant difference in the response of mode 1. Note that, for this problem, the unsteady aerodynamics (both linear and nonlinear) are updated at every outer-loop iteration. Also, the nonlinear portion of the damping gradient term is, as in preceding examples, not included in the computations.

As a final comparison, the resulting design obtained using the linear aerodynamics is taken and a flutter analysis performed using nonlinear unsteady aerodynamics to determine if, in fact, the linear design is conservative for this case. The flutter velocity obtained using the linear final design and nonlinear aerodynamics is 15,031 in./s with a flutter frequency of 19.42 Hz. This does satisfy the flutter constraint but only by about 3% with an 18.75% weight penalty. The possibility does exist that if a flutter constraint of 15,031 in./s is imposed on

Table 3 Fighter wing linear and nonlinear final designs for flutter constraints[a]

Global design variable	Local design variable	Linear final physical value	Nonlinear final physical value	% difference between linear and nonlinear
1	CROD 101–131	0.012 in.^{2}	0.009 in.^{2}	−26.92
2	CSHEAR 309, 310, 312, 314, 316, 318, 312, 324, 328, 332	0.019 in.	0.019 in.	+0.00
3	CSHEAR 311, 313, 315, 317, 319, 322, 325, 329, 333	0.016 in.	0.016 in.	+0.00
4	CSHEAR 320, 323, 326, 330, 334	0.062 in.	0.015 in.	−76.21
5	CSHEAR 327, 331, 335	0.045 in.	0.045 in.	−10.00
6	CROD 134–153	0.106 in.^{2}	0.159 in.^{2}	+50.36
7	CROD 164–181	0.075 in.^{2}	0.083 in.^{2}	+10.76
8	CROD 188–197	0.075 in.^{2}	0.750 in.^{2}	+0.00
9	CROD 204–209	0.625 in.^{2}	0.625 in.^{2}	+0.00
10	CSHEAR 340–361	0.120 in.	0.120 in.	+0.00
11	CTRMEM 1, 2	0.031 in.	0.028 in.	−10.47
12	CTRMEM 23, 24	0.024 in.	0.023 in.	−3.60
13	CTRMEM 43, 44	0.010 in.	0.009 in.	−9.36
14	CTRMEM 55, 56	0.060 in.	0.060 in.	+0.00
15	CQDMEM1 3–22	0.343 in.	0.067 in.	−80.59
16	CQDMEM1 25–42	0.282 in.	0.282 in.	+0.00
17	CQDMEM1 45–54	0.120 in.	0.120 in.	+0.00
18	CQDMEM1 57–62	0.060 in.	0.060 in.	+0.00
19	CSHEAR 300, 336	0.202 in.	0.203 in.	+0.00
20	CSHEAR 301–304, 337	0.180 in.	0.180 in.	+0.00
21	CSHEAR 305, 306, 338	0.135 in.	0.087 in.	+35.56
22	CSHEAR 307, 308, 339	0.075 in.	0.075 in.	+0.00
23	CROD 132, 133, 154, 155	2.188 in.^{2}	2.188 in.^{2}	+0.00
24	CROD 156–163, 182, 183	0.140 in.^{2}	0.150 in.^{2}	+6.58
25	CROD 184–187, 198, 199	1.313 in.^{2}	1.312 in.^{2}	+0.00
26	CROD 200–203, 210, 211	1.100 in.^{2}	1.100 in.^{2}	+0.00

[a]$M_\infty = 0.93$, $\alpha_0 = 0.5$ deg

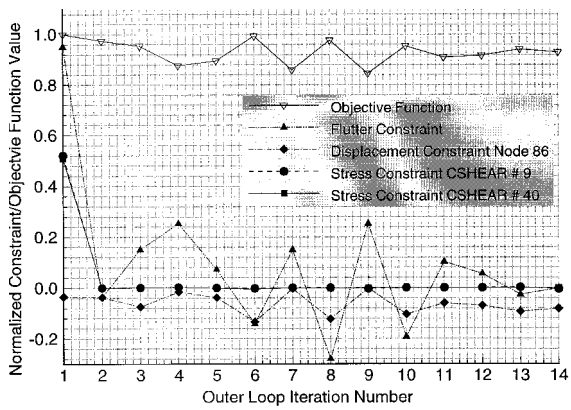

Fig. 11 Fighter wing objective function and critical constraint history. $M_\infty = 0.93$, $\alpha_0 = 0.50$ deg.

the nonlinear design, the weight would increase. This is probably true, but it is highly unlikely that the increase would be on the order of 18%.

Fighter Wing Case 3: $M_\infty = 0.93$, $\alpha_0 = 0.5$ deg, Flutter, Stress, and Displacement Constraints

As a final case, stress and displacement constraints are added to the preceding example ($M_\infty = 0.93$, $\alpha_0 = 0.5$ deg, flutter constraints). Also, only nonlinear unsteady aerodynamics are considered. For this example, a single static load case is added. This consists of an upward total force of 32,000 lb distributed evenly at the wingtip (nodes 81, 82, 85, 86). The displacement constraints specified are that the upward vertical displacements at all nodes do not exceed 17.0 in. Also, the allowable tension, compression, and shear stress limits are 60,000, 60,000, and 40,000 psi, respectively. Using these stress allowables, a von Mises stress constraint as defined by ASTROS (Ref. 15) is applied to all shear panels, skins, spar caps, and rib caps. The redesign produced a converged solution in 14 outer-loop iterations, to an objective function (the designed portion of the system) of 462.91 lb, 7% less than the initial value and 8.4% greater than the case with flutter constraints alone. Figure 11 plots the normalized constraint and objective function histories for the redesign process. This indicates that both the flutter and stress constraints are violated at the initial design. It also shows that, at the final design, the sizing is driven by the flutter and stress constraints, with the displacement constraint being approximately 8% feasible.

Concluding Remarks

A methodology for including transonic flutter requirements in the preliminary automated structural design environment is developed and tested. The problem of minimizing structural weight while satisfying behavioral constraints is stated in nonlinear mathematical programming form and solved using a gradient-based optimizing technique. The structure is modeled using finite elements, and the associated design variables consist of structural properties such as thicknesses of skins, spars, and ribs; cross-sectional areas of posts and spar and rib caps; and concentrated masses. The method requires the transonic unsteady aerodynamics be represented in the frequency or Laplace domain. In this work, the IRM is used to transform time–domain aerodynamics found by solving the TSD equations into the Laplace domain. The indicial responses are performed about static aeroelastic equilibriums found using the TSD equations for the steady aerodynamics. Once in the Laplace domain, the unsteady aerodynamics are used to determine system dynamic stability by the *p*-method and to develop semianalytic equations for the constraint sensitivities. Once the constraint values and sensitivities are obtained, the redesign can be performed. This is accomplished by solving the nonlinear mathematical programming problem. Using linear TSA of the objective function, constraints, objective-function gradients, and constraint gradients, an approximate problem is constructed. The MMFD is used to solve the approximate

problem, with move limits imposed on the design variables to ensure the variables do not stray too far from the point of linearization. Additionally, constraint screening and design variable linking techniques are employed to reduce the number of constraints and design variables submitted to the optimizer.

When performing the design studies, several of the test cases are solved using both linear and nonlinear aerodynamics. This is done so that the effects of using nonlinear as opposed to linear aerodynamics can be evaluated. The conclusion that can be drawn from these comparisons is that the designs are different. The differences occur in both the sizes of the members and the distribution of the material.

Note that in all design cases, the nonlinear term in the damping gradient is not computed, even though static aeroelastic equilibriums are used as starting points for the indicial responses. Also, depending on the problem, the unsteady aerodynamics are not recalculated at every exact constraint evaluation. Generally, they are recomputed at every other outer-loop iteration. This resulted in a considerable computational savings. All example cases converged in fewer than 30 outer-loop iterations, and most converged in fewer than 15. The move limits on the design variables varied anywhere from 1 to 200%, depending on the problem and the iteration. A variable move limit strategy was employed. This entailed allowing large move limits in the initial iterations and then reducing the move limits as the design approached the optimum.

Various state-of-the-art computational methods are adopted and systemized for predicting transonic unsteady aeroelastic responses economically and for searching for optimal designs in an efficient and automated fashion. It is hoped that these proposed systematic approaches and the demonstrated examples will add to the benchmark literature, so that they can be used and compared by the engineers who are working in the future environment, where interdisciplinary design becomes increasingly important and inevitable.

References

[1]Neill, D. J., Johnson, E. H., and Herendeen, D. L., "Automated STRuctural Optimization System (ASTROS)," *User's Manual*, Vol. 2, U.S. Air Force Wright Aeronautical Labs., TR-883028, April 1988.

[2]Johnson, E. H., and Reymond, M. A., "Multidisciplinary Aeroelastic Analysis and Design Using MSC/NASTRAN," AIAA Paper 91-1097, April 1991.

[3]Nicot, P., and Becus, G. A., *ELFINI Aeroelasticity Module—General Introduction Manual*, AMD-BA, 1988.

[4]Kneppe, G., "MBB-LAGRANGE—Structural Optimization System for Space and Aircraft Structures," Messerschmitt-Bölkow-Blohm, Rept. S/PUB/406, Munich, Germany, June 1990.

[5]Bartholomew, P., and Vinson, S., "Stars Mathematical Foundations," *International Series of Numerical Mathematics*, Birkhäuser Verlag, Basel, Switzerland, 1993, pp. 251–283.

[6]Brama, T., "The Structural Optimization System OPTSYS—Current Status and Applications," AGARD Rept. 784, National Technical Information Service, Springfield, VA, Feb. 1992, pp. 6-1–6-9.

[7]Ding, H., Sun, Xiasheng, Sun, Xianxue, Li, G., Wu, G., and Pan, B., "Engineering Optimization of Aeronautical Structures," International Council of the Aeronautical Sciences, 92-6.3R, pp. 599–607.

[8]"ARGON-Program Complex," Central Aerohydrodynamic Inst., Russia.

[9]Kapania, R. K., "Sensitivity Analysis of Dynamic Aeroelastic Responses," AGARD Rept. 784, Feb. 1992, pp. 3-1–3-12.

[10]Kapania, R. K., Issac, J. C., and Barthelemy, J. F. M., "Sensitivity Analysis of Flutter Response of a Typical Section and a Wing in Transonic Flow," AIAA Paper 93-1646, April 1993.

[11]Leishman, J. G., and Nguyen, K. Q., "State-Space Representation of Unsteady Airfoil Behavior," *AIAA Journal*, Vol. 28, No. 5, 1990, pp. 836–844.

[12]Stephenson, A. M., "Linearized Transonic Aerodynamics for Aircraft Design," M.S. Thesis, Univ. of Dayton, Dayton, OH, July 1992.

[13]Kolonay, R. M., "Transonic Unsteady Aeroelastic Analysis for the Multidisciplinary Design Environment," AIAA Paper 95-1285, April 1995.

[14]Vanderplaats, G. N., *Numerical Optimization Techniques for Engineering Design: With Applications*, McGraw–Hill, New York, 1984.

[15]Johnson, E. H., and Venkayya, V. B., "Automated STRuctural Optimization System (ASTROS)," *Theoretical Manual*, Vol. 1, U.S. Air Force Wright Aeronautical Labs., TR-883028, Dec. 1988.

[16]Hajela, P., "A Root Locus Based Flutter Synthesis Procedure," AIAA Paper 83-0063, Jan. 1983.

[17]Kolonay, R. M., "Sensitivity Analysis for Transonic Unsteady Aeroelastic Constraints," AIAA Paper 96-1338, April 1996.

[18]Schmit, L. A., and Miura, H., "Approximation Concepts for Efficient Structural Synthesis," NASA CR-2552, March 1976.

[19]Batina, J. T., "A Finite-Difference Approximate-Factorization Algorithm for Solution of the Unsteady Transonic Small-Disturbance Equation," NASA TP 3129, Jan. 1992.

[20]Harder, R. L., and Desmarais, R. N., "Interpolation Using Surface Splines," *Journal of Aircraft*, Vol. 9, No. 2, 1972, pp. 189–191.

[21]Borland, C. J., "XTRAN3S-Transonic Steady and Unsteady Aerodynamics for Aeroelastic Applications," Vol. 1, U.S. Air Force Wright Aeronautical Labs., TR-85-3124, Jan. 1986.

[22]Striz, A. G., and Venkayya, V. B., "Influence of Structural and Aerodynamic Modeling on Optimization with Flutter Constraint," *Proceedings of the 3rd USAF/NASA Symposium on Recent Advances in Multidisciplinary Analysis and Optimization*, Anamet Labs., Inc., Hayward, CA, 1990, pp. 431–438.